Archives of Craniofacial Surgery
Arch Craniofac Surg Vol.27 No.2, 80-87
https://doi.org/10.7181/acfs.2026.0044

Original Article

Transnasal balloon-assisted posterior ridge restoration for inferior orbital wall fractures

Sungyeon Kim, Hong Bae Jeon, Hyonsurk Kim, Dong Hee Kang

Department of Plastic and Reconstructive Surgery, Dankook University Hospital, Cheonan, Korea

Background: We aimed to evaluate the clinical efficacy of primary bone restoration with transnasal balloon-assisted support for inferior orbital wall fractures and compared it with the efficacy of conventional alloplastic reconstruction.
Methods: A total of 85 patients were included in this study. Of them, 25 underwent transconjunctival reconstruction with alloplastic implants (Group A), whereas the remaining 60 underwent primary bone reduction with transnasal balloon-assisted support (Group B). Postoperative outcomes were evaluated based on Hertel exophthalmometry, the orbital volume ratio (OVR) calculated from 6-month follow-up computed tomography (CT) scans, and a curvature analysis of the posterior orbital floor contour on sagittal CT images.
Results: Both groups showed significant postoperative improvements in OVR (from 109.23% to 103.07% in Group A; from 111.17% to 103.27% in Group B; $p<0.001$). The mean change in the Hertel scale was –0.20 mm in Group A and –0.43 mm in Group B, with no statistically significant difference between the groups ($p>0.05$). No significant difference was observed in the magnitude of volume reduction between Groups A (6.16%) and B (7.90%; $p=0.296$). Curvature analysis demonstrated a significantly smaller absolute curvature difference between the operated and contralateral sides in Group B than in Group A (0.0136 vs. 0.0310; $p<0.001$).
Conclusion: Transnasal balloon-assisted primary bone restoration represents a reliable surgical alternative, facilitating the reconstruction of natural orbital floor contours while minimizing complications associated with conventional alloplastic implants.

Abbreviations: CT, computed tomography; OVR, orbital volume ratio

Keywords: Absorbable implants / Blowout fractures / Enophthalmos / Orbital implants

INTRODUCTION

Orbital wall fractures are a common consequence of midfacial trauma and often result from buckling or hydraulic mechanisms [1]. Disruption of the orbital bony envelope can alter the globe position and extraocular muscle function, leading to diplopia, motility restriction, and enophthalmos [2,3].

Orbital fracture surgery is primarily aimed at restoring both ocular function and projection by reconstructing the fractured orbital wall to its original shape [4,5]. However, the orbital cavity is not a simple conical structure; its medial and inferior orbital walls possess natural curvatures. Most fractures involve these two walls; the medial orbital wall curves inward into the orbit, whereas the inferior orbital wall features a crucial posterior ridge that significantly influences both globe projection and orbital volume [6,7].

Therefore, restoring the three-dimensional contour of the orbital wall is particularly challenging when using common conventional flat alloplastic implants [8,9]. These implants cannot fully replicate the native contour of the medial wall or the posterior ridge of the inferior wall, which makes precise restoration of the orbital volume and projection difficult. The posterior

Correspondence: Dong Hee Kang
Department of Plastic and Reconstructive Surgery, Dankook University Hospital, 201 Manghyang-ro, Dongnam-gu, Cheonan 31116, Korea
E-mail: dhkcool@daum.net

How to cite this article:
Kim S, Jeon HB, Kim H, Kang DH. Transnasal balloon-assisted posterior ridge restoration for inferior orbital wall fractures. Arch Craniofac Surg 2026;27(2):80-87. https://doi.org/10.7181/acfs.2026.0044

Received March 5, 2026 / Revised April 13, 2026 / Accepted April 20, 2026

www.e-acfs.org
pISSN 2287-1152
eISSN 2287-5603

bony ridge serves as a critical anatomical landmark, and accurate restoration of the natural shape of the orbital wall is essential for favorable surgical outcomes and restoration of the natural orbital wall contour [10,11].

To address this limitation, a technique for reconstructing the inferior orbital wall using temporary transnasal balloon support within the maxillary sinus has been proposed. This method facilitates the effective restoration of the posterior ridge using the patient's primary bone fragment [12]. Building upon this concept, the present study performed a comparative analysis between patients who underwent orbital floor reconstruction with conventional alloplastic implants and those treated with primary bone restoration combined with resorbable implants and balloon support. Clinical outcomes were assessed over a 6-month follow-up period to evaluate the efficacy of this technique.

METHODS

Participant selection

This study was approved by the Institutional Review Board and conducted in accordance with the principles of the Declaration of Helsinki. We retrospectively reviewed the medical records of patients who underwent surgical treatment for orbital fractures between June 2020 and June 2024. Of the 602 patients identified, 150 with complex orbital fractures and 167 with isolated medial orbital wall fractures were excluded. Among the remaining 285 patients with inferior orbital wall fractures, we further excluded one patient with bilateral inferior orbital wall fractures and 79 patients who did not undergo postoperative Hertel exophthalmometry. Consequently, 85 patients were included in this study (Fig. 1). Prior to surgery, both conventional alloplastic implant techniques and primary bone restoration technique with transnasal balloon support was explained to each patient. The surgical method was then selected based on the patient's preference. Accordingly, 25 patients underwent the approach using an alloplastic implant (Group A, control group), while 60 received primary bone restoration via the transnasal balloon technique (Group B, experimental group).

Ophthalmic and radiologic examination

The indications for surgical intervention were determined based on the presence of at least one of the following criteria: (1) limited extraocular muscle motility, (2) radiologic confirmation of a large orbital floor defect exceeding 2 cm² on computed tomography (CT), (3) subjective complaint of diplopia, or (4) clinically evident enophthalmos greater than 2 mm. Before surgery, all patients underwent standardized ophthalmological evaluation, including assessment of diplopia, extraocular muscle motility, and enophthalmos. The degree of enophthalmos

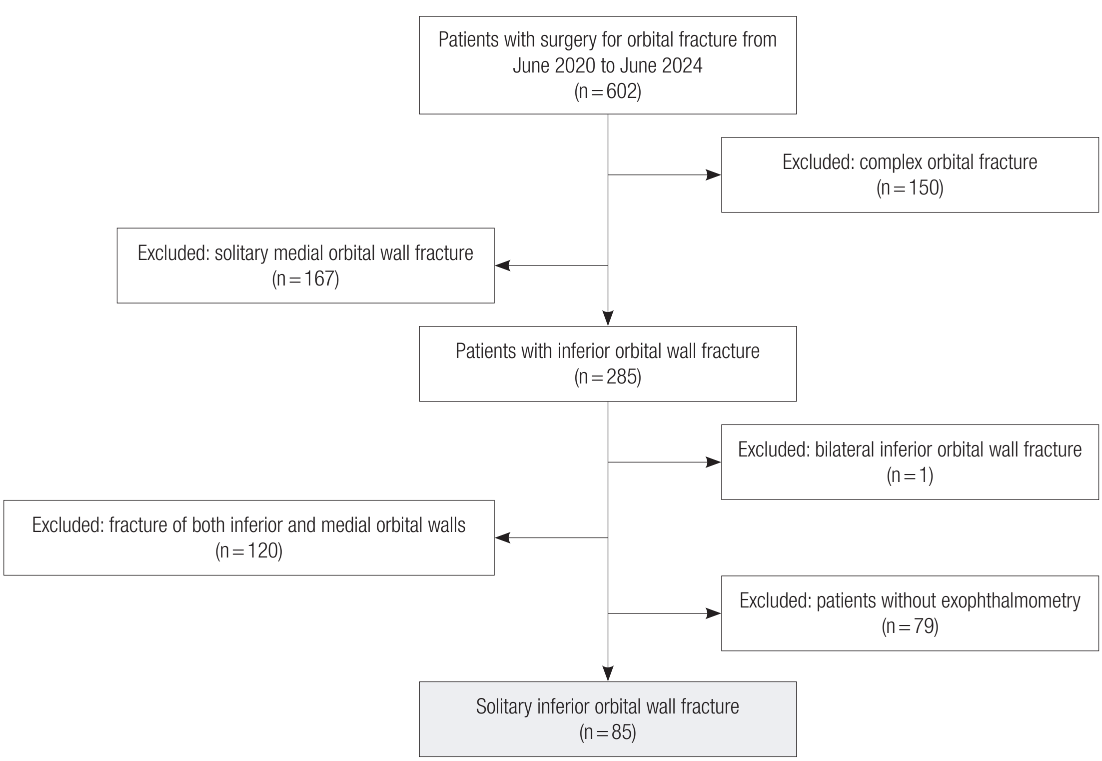

Fig. 1. Flowchart of patient selection and exclusion criteria.

was measured using a Hertel exophthalmometer (Inami). Measurements were obtained for 1 day before surgery to minimize the influence of acute posttraumatic edema. Preoperative and postoperative orbital CT scans were performed, with postoperative scans obtained at least 6 months after surgery. Scans were acquired in 1-mm axial and coronal slices using a multidetector CT system. Orbital volume was quantified using image post-processing software (Rapidia; Infinitt), which allowed manual segmentation of the orbital boundaries on each CT slice. The OVR was calculated by dividing the volume of the affected orbit by that of the contralateral, uninjured orbit. This approach provided an individualized comparison, accounting for inter-participant anatomical variations. Postoperative OVR was calculated using the same formula at the 6-month follow-up, coinciding with the stabilization of orbital soft tissue and scar remodeling.

Curvature assessment of the restored posterior orbital floor contour

Curvature of the restored posterior orbital floor contour was approximated on postoperative sagittal CT using a three-point circumcircle method (Fig. 2). Measurements were performed on the sagittal slice passing through the center of the orbital floor defect, where the restored posterior contour was best visualized. Three anatomically identifiable points were selected along the contour: the apex of the posterior convexity, the anterior transition point of the reconstructed floor contour, and the posterior end of the restored cortical contour at the posterior ridge. Curvature was approximated as the reciprocal of the circumradius defined by these three points and expressed in mm^{-1} after conversion using CT pixel spacing [13,14].

Surgical techniques

All procedures were performed under general anesthesia. Initially, a forced duction test was conducted to assess passive globe motility. A transconjunctival incision was made in the inferior fornix approximately 3 mm inferior to the tarsal plate. Preseptal and subperiosteal dissections were performed to expose the infraorbital rim and orbital floor, clearly delineating the fracture margins. Herniated orbital tissues were reduced under direct visualization, and the forced duction test was repeated to ensure unrestricted extraocular movement. Upon completion, the periosteum and conjunctiva were closed with absorbable sutures.

Group A: alloplastic orbital floor reconstruction

In Group A, orbital floor defect was reconstructed using a porous polyethylene implant (Synpor; DePuy Synthes). The implant was meticulously trimmed to match the size and contour of the defect and was positioned to restore structural support to the orbital floor. Forced duction testing was repeated after placement to confirm the absence of mechanical entrapment.

Group B: primary bone reduction and transnasal balloon-assisted posterior ridge support

In Group B, the surgical strategy focused on anatomical reduction of the primary bony fragments. Following nasal decongestion with epinephrine-soaked pledgets, 2% lidocaine with

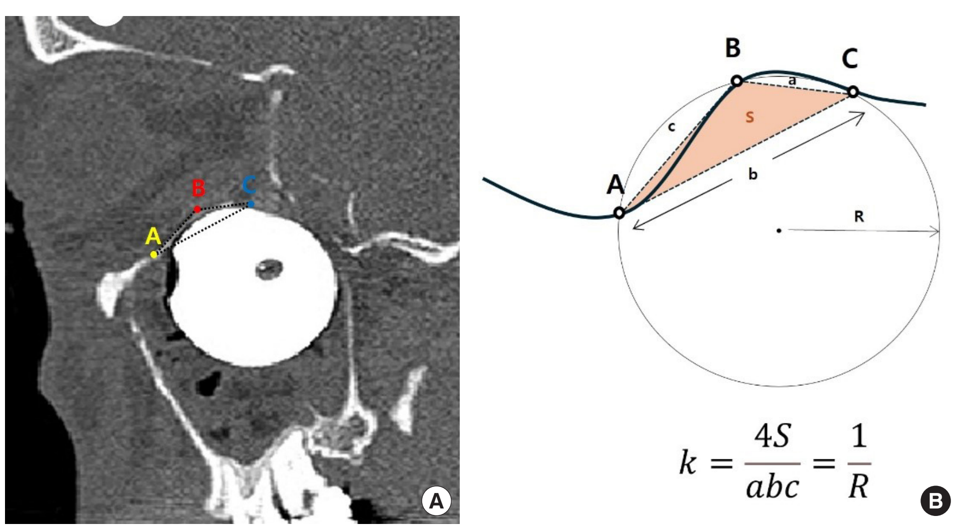

$$k = \frac{4S}{abc} = \frac{1}{R}$$

Fig. 2. Three-point curvature approximation of the restored posterior orbital floor contour on postoperative sagittal CT. (A) Postoperative sagittal CT image showing the three selected points along the restored posterior orbital floor contour: A, anterior transition point; B, apex of the posterior convexity; and C, posterior end of the restored cortical contour at the posterior ridge. (B) Schematic illustration of the three-point circumcircle method. Curvature was approximated as κ=1/R, where R=abc/4S. CT, computed tomography.

1:100,000 epinephrine was infiltrated into the anterior root of the middle turbinate and uncinate processes. The maxillary sinus was accessed through the natural ostium using a curved Freer elevator. Under direct visualization from the orbital side, the displaced bone fragments were reduced, and the herniated contents were repositioned. Subsequently, a 14- or 16-Fr Foley catheter was advanced transnasally into the maxillary sinus via the ostium. The balloon was inflated with a mixture of saline and contrast dye to provide stable support for the reduced bony fragments and posterior orbital floor ridge, thereby restoring the physiologic contour. The optimal inflation volume was determined under direct visualization to ensure proper alignment of the fragments with the posterior ridge. In cases where the residual orbital floor defect exceeded 0.5×0.5 cm^2 after reduction of the primary bony fragments, an additional thermoplastic resorbable mesh plate was applied. Following placement, warm saline irrigation was used to facilitate molding of the mesh to the contour of the orbital floor.

Statistical analysis

Statistical analyses were performed using the SPSS software (version 20.0; IBM Corp.). Continuous variables, including OVR and Hertel scale measurements, were compared between the two groups using the Mann-Whitney *U* test. Intragroup longitudinal changes (preoperative vs. postoperative) were evaluated using the Wilcoxon signed-rank test. Statistical significance was defined as $p < 0.05$.

RESULTS

In total, 85 patients with isolated inferior orbital wall fractures were included in this study: 25 in Group A and 60 in Group B. Preoperatively, 52 patients (12 in Group A and 40 in Group B) presented with enophthalmos, and 11 patients (3 in Group A and 8 in Group B) exhibited limited extraocular movement. Following reconstruction, all patients were free of ocular symptoms, including diplopia and restricted ocular motility.

The mean preoperative Hertel measurements were –0.68 mm in Group A and –0.79 mm in Group B, with postoperative values improving to –0.48 mm and –0.36 mm, respectively (Table 1). The mean change (Δ) in the Hertel scale was –0.20 mm for Group A and –0.43 mm for Group B, with no statistically significant differences observed between the preoperative and postoperative Hertel measurements within either group ($p =$ 0.465 for Group A and $p = 0.280$ for Group B). Furthermore, no significant intergroup difference was observed in the degree of improvement in the Hertel scale (Table 1).

Regarding the OVR, the mean preoperative OVR was 109.23% in Group A and 111.17% in Group B. Postoperatively, these ratios decreased to 103.07% in Group A and 103.27% in Group B, representing volume reductions of 6.16% and 7.90%, respectively. These intragroup improvements were statistically significant ($p < 0.05$, Wilcoxon signed-rank test). However, the difference in the magnitude of volume reduction between the two groups was not statistically significant ($p = 0.296$, Mann-Whitney *U* test) (Table 1).

Table 1. Comparison of exophthalmometry, orbital volume ratio, and contour curvature between the two groups

Variable	Group A (n = 25)	Group B (n = 60)	*p*-value
Hertel scale (mm)			
Preoperative	–0.68	–0.79	0.183
Postoperative	–0.48	–0.36	0.282
Hertel change	–0.20	–0.43	0.161
p-value	0.465	0.280	
Orbital volume ratio (%)			
Preoperative	109.23	111.17	0.217
Postoperative	103.07	103.27	0.757
Volume change	6.16	7.90	0.296
p-value	< 0.001[a]	< 0.001[a]	
Posterior ridge curvature (mm^{-1})			
Contralateral	0.0480	0.0430	0.418
Postoperative	0.0199	0.0356	< 0.001[b]
Curvature difference	0.0310	0.0136	< 0.001[b]
p-value	< 0.001[a]	0.148	

Values are presented as mean. Change values represent mean differences.
[a]Significant difference, $p < 0.05$ (Wilcoxon signed-rank test); [b]Significant difference, $p < 0.05$ (Mann-Whitney *U* test).

Posterior orbital floor contour curvature was compared between the operated and contralateral sides in each group (Table 1). In Group A, postoperative curvature differed significantly from contralateral curvature (0.0199 vs. 0.0480; $p < 0.001$), whereas in Group B, no significant difference was observed between the operated and contralateral sides (0.0356 vs. 0.0430; $p = 0.148$). In addition, the absolute difference between postoperative and contralateral curvature was significantly smaller in Group B than in Group A (0.0136 vs. 0.0310; $p < 0.001$).

DISCUSSION

Accurate restoration of orbital floor curvature is essential for successful reconstruction. The orbital floor follows a characteristic "lazy S" contour, featuring a pronounced posteromedial convex ridge (the posterior ridge) that maintains the three-dimensional integrity of the orbit [5,6]. Failure to restore this curvature may result in persistent enophthalmos, hypoglobus, or diplopia, even when the bony defect is adequately covered [6]. Therefore, orbital fracture repair must focus on closing the defect and reestablishing this native curvature, particularly the posterior convexity, to achieve precise anatomical and functional outcomes.

Despite their malleability, conventional alloplastic implants typically feature a relatively flat configuration, which limits accurate reproduction of physiological posterior bulging [7]. This limitation is compounded by soft tissue prolapse and posttraumatic edema, which can obscure the posterior defect margin. In large fractures, secure placement near the posterior ridge is challenging, and inadequate restoration increases the risk of postoperative enophthalmos.

In the present study, orbital floor restoration using primary bone fragments combined with a transnasal balloon support effectively restored the natural contour (Figs. 3-5). The balloon, inserted via the maxillary ostium, provided temporary support to the orbital floor. This approach enabled a more anatomically accurate three-dimensional reduction of the posterior ridge compared with conventional implant-based methods. It also facilitated the use of the patient's primary bone fragments, potentially reducing implant-related complications such as malposition or infection [7].

The objective data from our study supported the efficacy of this technique. Regarding enophthalmos correction, the mean change in the Hertel scale was –0.20 mm for Group A ($n=25$) and –0.43 mm for Group B ($n=60$). Despite these improvements, no statistically significant intragroup differences were observed between the preoperative and postoperative measurements in both groups ($p=0.465$ for Group A; 0.280 for Group B),

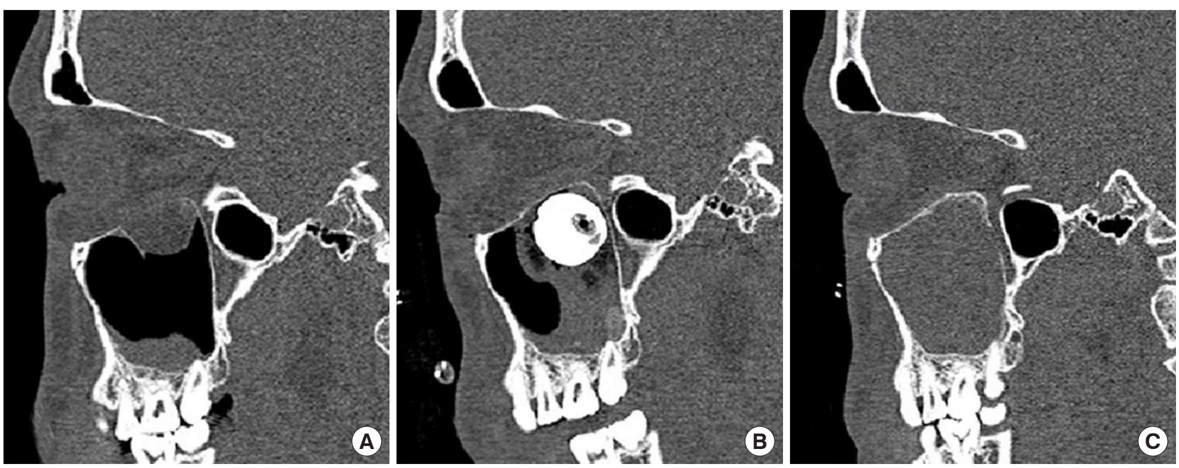

Fig. 3. A 25-year-old man with a right inferior orbital wall fracture who underwent posterior ridge restoration with transnasal balloon-assisted support. (A) Preoperative computed tomography (CT) scan. (B) Immediately postoperative CT scan demonstrating balloon support within the maxillary sinus. (C) Six-month postoperative CT scan showing restoration of the posterior orbital floor contour.

Fig. 4. A 49-year-old man with a left inferior orbital wall fracture who underwent posterior ridge restoration with transnasal balloon-assisted support. (A) Preoperative computed tomography (CT) scan. (B) Immediately postoperative CT scan demonstrating balloon support within the maxillary sinus. (C) Six-month postoperative CT scan showing restoration of the posterior orbital floor contour.

and no significant between-group difference was noted. Regarding OVR, both groups achieved significant volume reduction. The mean OVR decreased from 109.23% to 103.07% in Group A and from 111.17% to 103.27% in Group B, showing statistically significant intragroup improvements ($p < 0.001$). Regarding intergroup comparison, the volume reduction was 6.16% in Group A and 7.90% in Group B. The between-group difference in volume change was not statistically significant ($p = 0.296$), suggesting that the transnasal balloon technique was as effective as conventional alloplastic implants in restoring orbital volume.

An absorbable mesh plate was used when residual defects exceeded 0.5×0.5 cm^2 and provided support along with balloon until the orbital wall healed [4]. By providing temporary support, balloon assistance may reduce the risk of implant buckling, sagging, or displacement into the maxillary sinus, as reported with conventional techniques [1,4]. However, technique-specific limitations were identified. In Group A, posterior implant displacement occurred in two cases with large fractures (Fig. 6), highlighting the difficulty of seating flat implants. In Group B, three patients showed mild downward displacement at 6 months (Fig. 7), indicating that delayed settling may occur in severe defects and underscoring a potential need to optimize the duration of balloon support. However, since these patients did not exhibit clinically significant symptoms such as persistent diplopia or restricted eye movement, reoperation was not performed, and only follow-up observation was conducted.

Although patient-specific three-dimensional printed implants exist, they remain alloplastic. The combination of primary bone restoration and balloon buttressing is particularly favorable for

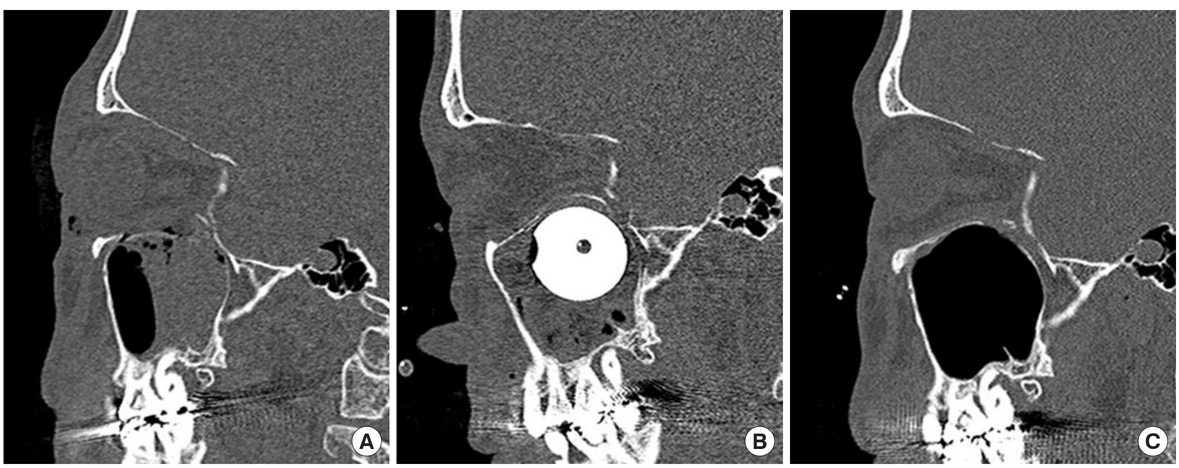

Fig. 5. A 42-year-old man with a left inferior orbital wall fracture who underwent posterior ridge restoration with transnasal balloon-assisted support. (A) Preoperative computed tomography (CT) scan. (B) Immediately postoperative CT scan demonstrating balloon support within the maxillary sinus. (C) Six-month postoperative CT scan showing restoration of the posterior orbital floor contour.

Fig. 6. A 29-year-old man with a large right inferior orbital wall fracture showing postoperative alloplastic implant displacement. (A) Preoperative computed tomography (CT) scan. (B) Postoperative CT scan showing posterior displacement of the alloplastic implant into the maxillary sinus. As no clinically significant ocular symptoms developed, the patient was managed with observation without revision surgery.

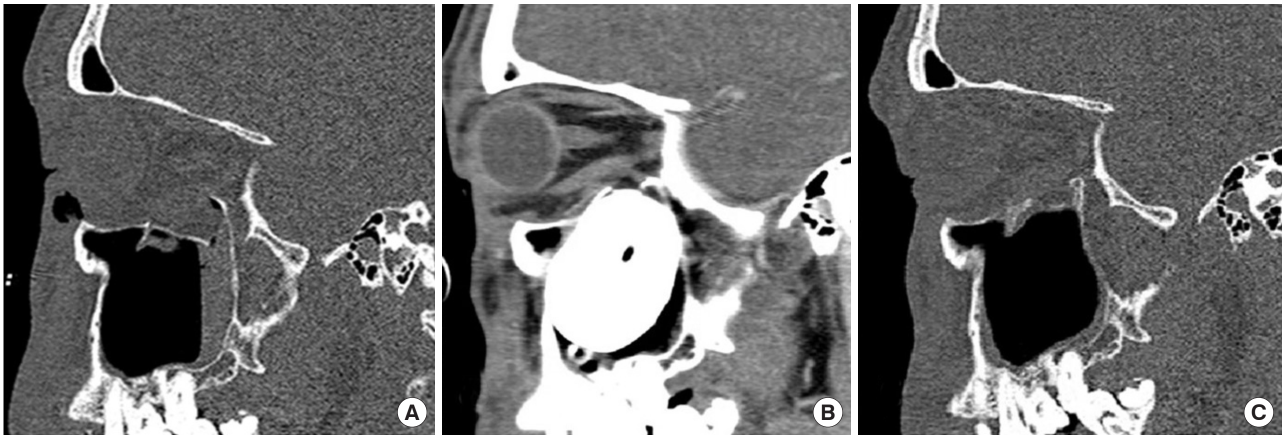

Fig. 7. A 41-year-old man with a right inferior orbital wall fracture showing posterior ridge subsidence at 6-month follow-up after balloon removal. (A) Preoperative computed tomography (CT) scan. (B) Immediate postoperative CT scan demonstrating balloon support. (C) Six-month postoperative CT scan showing posterior ridge subsidence. The transnasal balloon was removed on postoperative day 7, and no enophthalmos was observed at the 6-month follow-up.

patients at a higher risk of infection because it avoids permanent foreign bodies. In our series, the balloon was generally maintained for 7 days with extension by 1–2 days in cases of larger defects with less-secure fragment stability, balancing the need for stabilization against patient morbidity. Although patients experienced minor discomfort due to the maintenance of the catheter, no complications were observed. However, there is currently no balloon device specifically designed for this procedure, and patient discomfort could be improved if a dedicated balloon system is developed in the future.

In conclusion, this study demonstrates that combining primary bone restoration with transnasal balloon-assisted support facilitates significant anatomical curvature recovery in the reconstruction of inferior orbital wall fractures. Although improvements in exophthalmos and OVR did not reach statistical significance, this technique serves as a reliable alternative capable of restoring natural floor contours while minimizing complications inherent to conventional alloplastic implants. To further validate its clinical efficacy, subsequent studies involving a larger sample size and longer follow-up periods are warranted.

NOTES

Conflict of interest

Dong Hee Kang is an editorial board member of the journal but was not involved in the peer reviewer selection, evaluation, or decision process of this article. No other potential conflicts of interest relevant to this article were reported.

Funding

None.

Ethical approval

The study was approved by the Institutional Review Board of Dankook University Hospital (IRB No. DKUH 2026-02-001-002) and performed in accordance with the principles of the Declaration of Helsinki.

Patient consent

The patients provided written informed consent for the publication and use of their images.

ORCID

Sungyeon Kim https://orcid.org/0000-0003-4342-9088
Hong Bae Jeon https://orcid.org/0000-0003-2412-4537
Hyonsurk Kim https://orcid.org/0000-0001-6576-8035
Dong Hee Kang https://orcid.org/0000-0002-6673-9655

Author contributions

Conceptualization: Dong Hee Kang. Data curation: Sungyeon Kim. Formal analysis: Sungyeon Kim. Methodology: Sungyeon Kim. Visualization: Sungyeon Kim. Writing–original draft: Sungyeon Kim. Writing–review & editing: Hong Bae Jeon, Hyonsurk Kim, Dong Hee Kang. Investigation: Sungyeon Kim, Hong Bae Jeon, Hyonsurk Kim. Supervision: Dong Hee Kang. Validation: Hong Bae Jeon, Hyonsurk Kim, Dong Hee Kang. All authors read and approved the final manuscript.

REFERENCES

1. Nagasao T, Miyamoto J, Jiang H, Tamaki T, Kaneko T. Interaction of hydraulic and buckling mechanisms in blowout fractures. Ann Plast Surg 2010;64:471-6.

2. Choi SH, Kang DH. Prediction of late enophthalmos using preoperative orbital volume and fracture area measurements in blowout fracture. J Craniofac Surg 2017;28:1717-20.
3. Kang DH. Orbital wall restoring surgery with primary orbital wall fragments in blowout fracture. Arch Craniofac Surg 2019; 20:347-53.
4. Oh SA, Aum JH, Kang DH, Gu JH. Change of the orbital volume ratio in pure blow-out fractures depending on fracture location. J Craniofac Surg 2013;24:1083-7.
5. Wong YC, Goh DSL, Yoong CSY, Ho C, Cai EZ, Hing A, et al. Mapping the posterior ledge and optic foramen in orbital floor blowout fractures. Arch Plast Surg 2023;50:370-6.
6. Chodankar NU, Dhupar V, Vijay V, Fernandes N. Surgical anatomy in orbital fractures: a surgeons perspective. J Maxillofac Oral Surg 2024;23:462-74.
7. Duzgun S, Kayahan Sirkeci B. Comparison of post-operative outcomes of graft materials used in reconstruction of blow-out fractures. Ulus Travma Acil Cerrahi Derg 2020;26:538-44.
8. Nikunen M, Rajantie H, Marttila E, Snall J. Implant malposition and revision surgery in primary orbital fracture reconstructions. J Craniomaxillofac Surg 2021;49:837-44.
9. Lim NK, Kang DH, Oh SA, Gu JH. Orbital Floor Restoration Using the Transnasal Balloon Technique for Inferior Orbital Wall Fracture. Ann Plast Surg 2015;75:522-5.
10. Park JH, Kim I, Son JH. Incidence and management of retrobulbar hemorrhage after blowout fracture repair. BMC Ophthalmol 2021;21:186.
11. Gilliland GD, Gilliland G, Fincher T, Harrington J, Gilliland JM, Netto G, et al. Timing of return to normal activities after orbital floor fracture repair. Plast Reconstr Surg 2007;120:245-51.
12. Park JH, Kang DH, Jeon HB, Kim H. Orbital wall restoration with primary bone fragments in complex orbital fractures. Arch Craniofac Surg 2023;24:52-8.
13. Marciniak M, Gilbert A, Loncaric F, Fernandes JF, Bijnens B, Sitges M, et al. Septal curvature as a robust and reproducible marker for basal septal hypertrophy. J Hypertens 2021;39:1421-8.
14. Choi G, Cheng CP, Wilson NM, Taylor CA. Methods for quantifying three-dimensional deformation of arteries due to pulsatile and nonpulsatile forces: implications for the design of stents and stent grafts. Ann Biomed Eng 2009;37:14-33.